Coupled quantum electrodynamics in photonic crystal cavities towards controlled phase gate operations

2008 New J. Phys. 10 123013

(http://iopscience.iop.org/1367-2630/10/12/123013)

New Journal of Physics
The open-access journal for physics

Coupled quantum electrodynamics in photonic crystal cavities towards controlled phase gate operations

Y-F Xiao[1,2,3], J Gao[1], X-B Zou[2], J F McMillan[1], X Yang[1], Y-L Chen[2], Z-F Han[2], G-C Guo[2] and C W Wong[1]

[1] Optical Nanostructures Laboratory, Center for Integrated Science and Engineering, Solid-State Science and Engineering, and Department of Mechanical Engineering, Columbia University, New York, NY 10027, USA
[2] Key Laboratory of Quantum Information, University of Science and Technology of China, Hefei 230026, People's Republic of China
E-mail: yfxiao@gmail.com and cww2104@columbia.edu

New Journal of Physics **10** (2008) 123013 (13pp)
Received 25 June 2008
Published 9 December 2008
Online at http://www.njp.org/
doi:10.1088/1367-2630/10/12/123013

Abstract. In this paper, a scalable photonic crystal cavity array, in which single embedded quantum dots (QDs) are coherently interacting, is studied theoretically. Firstly, we examine the spectral character and optical delay brought about by the coupled cavities interacting with single QDs, in an optical analogue to electromagnetically induced transparency. Secondly, we then examine the usability of this coupled QD–cavity system for quantum phase gate operation and our numerical examples suggest that a two-qubit system with fidelity above 0.99 and photon loss below 0.04 is possible.

[3] Authors to whom any correspondence should be addressed.

Contents

1. Introduction

Cavity quantum electrodynamics (QED) describes a few atoms strongly coupling to quantized electromagnetic fields inside an optical cavity. Up to now, it is one of a few experimentally realizable systems in which the intrinsic quantum mechanical coupling dominates losses due to dissipation, providing an almost ideal system that allows the quantitative study of a dynamical open quantum system under continuous observation (for a review, see [1] and references therein). Over the past few years, theoretical and experimental studies have mainly focused on a single cavity interacting with atoms, and tremendous progress has been made ranging from strongly trapping single atoms [2] and deterministic generation of single-photon states [3], to observation of atom–photon quantum entanglement [4] and implementation of quantum communication protocols [5].

For more applications, current interest lies in the coherent interaction between distant cavities. The coherent interaction of cavity arrays has been studied as an optical analogue to electromagnetically induced transparency (EIT) in both theory [6, 7] and experiment [8, 9]. Coupled cavities can be utilized for coherent optical information storage, because they provide almost lossless guiding and coupling of light pulses at slow group velocities. When dopants such as atoms or quantum dots (QDs) interact with these cavities, the spatially separated cavities have been proposed for implementing quantum logic and constructing quantum networks [10, 11]. Recent studies also show a strong photon-blockade regime and photonic Mott insulator state [12], where the two-dimensional hybrid system undergoes a characteristic Mott insulator-to-superfluid quantum-phase transition at zero temperature [13]. Recently, it was shown that coupled cavities can also model an anisotropic Heisenberg spin-1/2 lattice in an external magnetic field [14]. The character of a coupled cavity configuration has also been studied using the photon Green function [15, 16].

2. Theoretical model

In this paper, using transmission theory, we study coherent interactions in a cavity array that includes N cavity–QD subsystems, with indirect coupling between adjacent cavities through a waveguide (figure 1). Recent experimental efforts have reported remarkable progress in solid-state cavities, such as ultra-high quality factors [17]–[19], observation of strong coupling

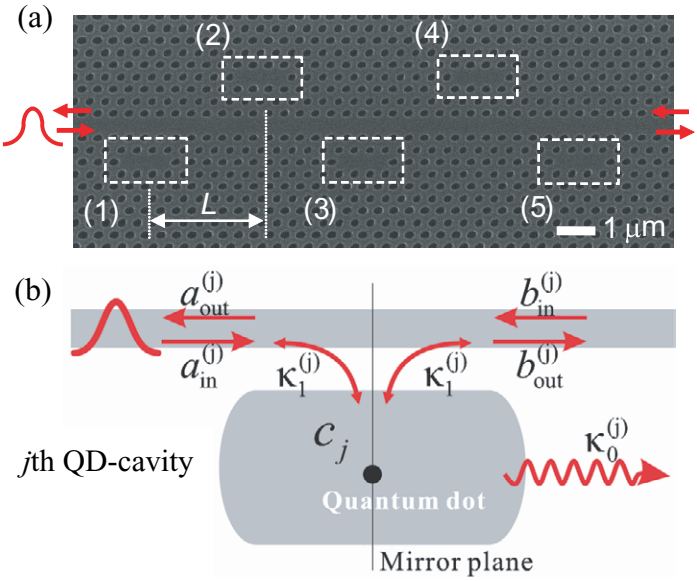

Figure 1. (a) Example scanning electronic micrograph of periodic waveguide–resonator structure containing N side-coupled cavities (h-polarized) at a distance L. (b) The jth QD–cavity subsystem.

and vacuum Rabi splitting [20, 21], transfer of single photons between two cavities [22], deterministic positioning of a cavity mode with respect to a QD [23], and controlling cavity reflectivity with a single QD [24].

First, we investigate a subsystem in which a single cavity interacts with an isolated QD. Here for simplicity we suppose that only a single resonance mode (h-polarized) is present in the cavity, although two-mode cavity–QD interactions have been considered earlier [25]. The cavity–QD–waveguide subsystem has mirror-plane symmetry, so that the mode is even with respect to the mirror plane. We can easily obtain the Heisenberg equations of motion [26, 27]

$$\frac{\mathrm{d}\hat{c}_j}{\mathrm{dt}} = -\mathrm{i}\left[\hat{c}_j, H_j\right] - \Gamma_j \hat{c}_j + \mathrm{i}\sqrt{\kappa_{1,j}}\left(\hat{a}_{\mathrm{in}}^{(\mathrm{j})} + \hat{b}_{\mathrm{in}}^{(\mathrm{j})}\right), \tag{1}$$

$$\frac{\mathrm{d}\hat{\sigma}_{-,j}}{\mathrm{dt}} = -\mathrm{i}\left[\hat{\sigma}_{-,j}, H_j\right] - \gamma_j \hat{\sigma}_{-,j} + \sqrt{\gamma_j'}\hat{\sigma}_j', \tag{2}$$

where c_j is the bosonic annihilation operator of the jth cavity mode with resonant frequency $\omega_{c,j}$. $\hat{a}_{\mathrm{in}}^{(\mathrm{j})}$ ($\hat{b}_{\mathrm{in}}^{(\mathrm{j})}$) and $\hat{a}_{\mathrm{out}}^{(\mathrm{j})}$ ($\hat{b}_{\mathrm{out}}^{(\mathrm{j})}$) describe the input and output fields in the left (right) port, respectively, with standard input–output relations $\hat{a}_{\mathrm{out}}^{(\mathrm{j})} = \hat{b}_{\mathrm{in}}^{(\mathrm{j})} + \sqrt{\kappa_{1,j}}\hat{c}_j$ and $\hat{b}_{\mathrm{out}}^{(\mathrm{j})} = \hat{a}_{\mathrm{in}}^{(\mathrm{j})} + \sqrt{\kappa_{1,j}}\hat{c}_j$. $2\Gamma_j$ represents total cavity decay with $\Gamma_j = (\kappa_{0,j} + 2\kappa_{1,j})/2$, where $\kappa_{0,j}$ is the intrinsic cavity decay rate and $\kappa_{1,j}$ the external cavity decay rate. $\hat{\sigma}_{-(+),j}$ is the descending (ascending) operator of the interacting two-level QD with transition frequency $\omega_{r,j}$. The variable γ_j is the total decay rate of the QD, including the spontaneous decay (at rate γ_{s}) and dephasing (at rate γ_{p}) in the excited state $|e\rangle$; H_j is the subsystem Hamiltonian: $H_j = \omega_{c,j}\hat{c}_j^{\dagger}\hat{c}_j + \omega_{r,j}\hat{\sigma}_{+,j}\hat{\sigma}_{-,j} + \left[g_j(\vec{r})\hat{\sigma}_{+,j}\hat{c}_j + \mathrm{h.c.}\right]$, where $g_j(\vec{r})$ is the coupling strength between the cavity mode and the dipolar transition $|g\rangle \leftrightarrow |e\rangle$. The variable $\hat{\sigma}_j'$ is the vacuum noise operator associated with the decay rate γ_j'.

In the weak excitation limit (excited by a weak monochromatic field or a single-photon pulse with frequency ω), by omitting the term that concerns the Langevin noises [27], the motion equations can be solved, with the transport relation in the frequency domain

$$\begin{pmatrix} \hat{b}_{\text{in}}^{(\text{j})}(\omega) \\ \hat{b}_{\text{out}}^{(\text{j})}(\omega) \end{pmatrix} = T_j \begin{pmatrix} \hat{a}_{\text{in}}^{(\text{j})}(\omega) \\ \hat{a}_{\text{out}}^{(\text{j})}(\omega) \end{pmatrix}. \tag{3}$$

Here the transport matrix reads

$$T_j = \frac{1}{\alpha_j + \kappa_{1,j} - \Gamma_j} \begin{pmatrix} -\kappa_{1,j} & \alpha_j - \Gamma_j \\ \alpha_j - \Gamma_j + 2\kappa_{1,j} & \kappa_{1,j} \end{pmatrix}, \tag{4}$$

where $\alpha_j = \text{i}\Delta_{c,j} + |g_j(\vec{r})|^2 / (\text{i}\Delta_{r,j} - \gamma_j)$, $\Delta_{c,j} = \omega - \omega_{c,j}$ $(\Delta_{r,j} = \omega - \omega_{r,j})$ represents the detuning between the input field and the cavity mode (QD transition). For convenience, we also define the cavity–QD detuning $\delta_j \equiv \omega_{c,j} - \omega_{r,j}$. The transport matrix can be regarded as a basic cell in cascading subsystems and as obtaining the whole transportation for the N-coupled cavity–QD system. The transport properties can thus be expressed as

$$\begin{pmatrix} \hat{b}_{\text{in}}^{(\text{N})}(\omega) \\ \hat{b}_{\text{out}}^{(\text{N})}(\omega) \end{pmatrix} = T_N T_0 \cdots T_0 T_2 T_0 T_1 \begin{pmatrix} \hat{a}_{\text{in}}^{(1)}(\omega) \\ \hat{a}_{\text{out}}^{(1)}(\omega) \end{pmatrix}, \tag{5}$$

where T_0 is the transport matrix via the waveguide with a propagation phase θ. When studying only the spectral character of the coupled QD–cavity interaction (section 3), we note that this is analogous to classical microwave circuit design [28], where the transmission and reflection characteristics from equation (5) can also be examined with coupled-mode theory with dipole terms inserted. Examining the spectral character first (section 3) helps to understand the coupled QD–cavity controlled quantum phase gate operation and performance (sections 4 and 5).

3. Spectral character of coupled QD–cavity arrays

To examine the physical essence, we need to first examine the spectral character of the coupled cavity–QD system. The reflection and transmission coefficients are defined as $r_{N1}(\omega) \equiv \hat{a}_{\text{out}}^{(1)}(\omega) / \hat{a}_{\text{in}}^{(1)}(\omega)$ and $t_{N1}(\omega) \equiv \hat{b}_{\text{out}}^{(N)}(\omega) / \hat{a}_{\text{in}}^{(1)}(\omega)$. In the following, we also assume that these cavities possess the same dissipation characteristics without loss of generality, i.e. $\kappa_{0,j} = \kappa_0$, $\kappa_{1,j} = \kappa_1$, $\kappa_1 = 50\kappa_0$ and $\Gamma_j = \Gamma$.

Figure 2(a) shows the transmission spectra of two coupled *empty* cavities (without QD) with different detuning $(\delta_{21} \equiv \omega_{c,2} - \omega_{c,1})$. When the two cavities are exactly resonant, a transmission dip is observed; with increasing the δ_{21}, a sharp peak exists at the center position between the two cavity modes. This is an optical analogue to the phenomenon of EIT in atomic vapors. We examine the classical optical analogue exactly through 3D finite-difference time-domain (FDTD) numerical simulations. Specifically, figures 2(b) and (c) show an example of the transmission and field distributions through the coherent interaction with two coupled *empty* cavities, where the resonance of one cavity is detuned by three cases: $\delta_{21} = 1.14\Gamma$, 1.26Γ and 1.49Γ. The optical transparency peak from the FDTD is broader than in figure 2(a) due to the finite grid-size resolution, and is observed on top of a background Fabry–Perot oscillation (due to finite reflections at the waveguide facets). The analogy and difference between an all-optical analogue to EIT and atomic EIT were recently discussed in [7].

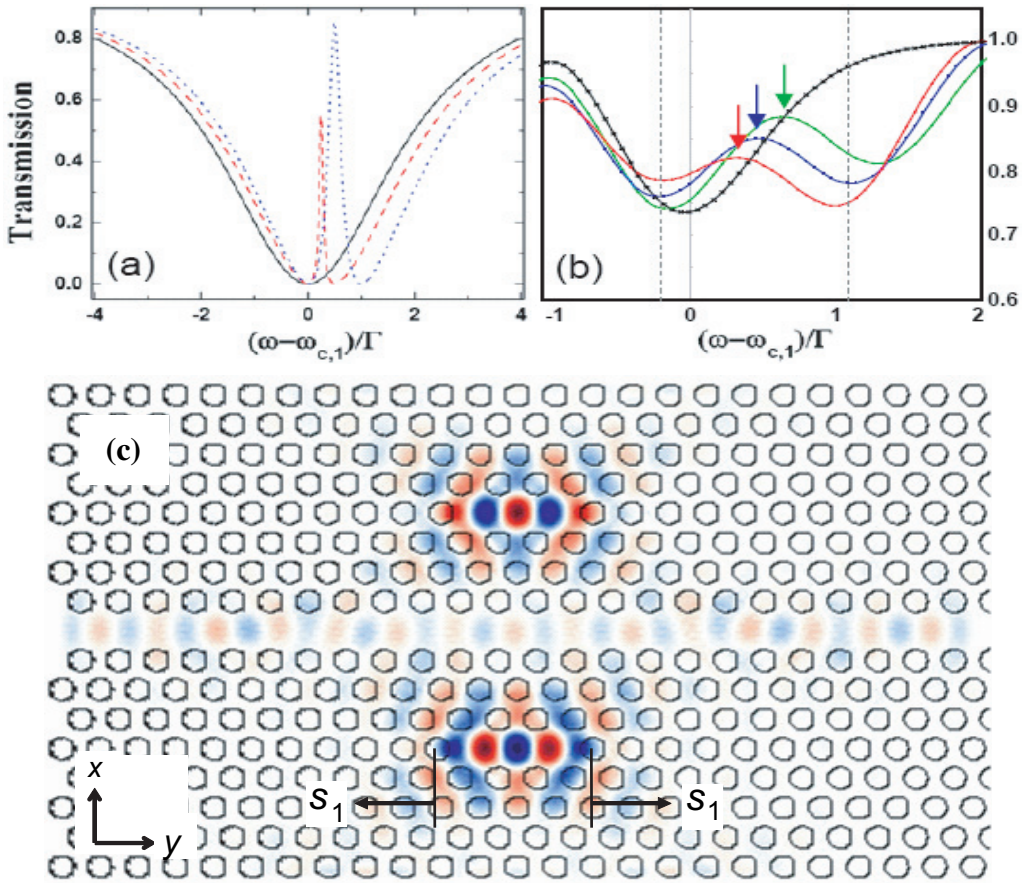

Figure 2. (a) and (b): Transmission spectra of two coupled empty cavities, where $\theta = 20\pi$. Solid, dashed and dotted lines describe the cases of $\delta_{21} = 0,\ \Gamma/2$ and Γ, respectively. (b) Numerical 3D FDTD simulations of the optical analogue of EIT in two coupled cavities ($\theta = 0$) for detunings 1.14Γ (red; $\Delta\varepsilon_{\text{cavities}} = 0.135$), 1.26Γ (blue; $\Delta\varepsilon_{\text{cavities}} = 0.160$) and 1.49Γ (green; $\Delta\varepsilon_{\text{cavities}} = 0.185$). The arrows denote the EIT peak transmissions. The dashed gray lines denote the two detuned individual resonances for the case of $s_1 = 0.05a$. The black curve is for a single cavity transmission for reference. (c) Example E_x-field distribution of coupled empty photonic crystal cavities.

Figure 3(a) (top) shows the spectral characteristics for the case where a single QD resonantly interacts with the first cavity, in the presence of QDs. When both cavities are resonant, there exist two obvious sharp peaks located symmetrically around $\omega = 0$ (for convenience, we define $\omega_{c,1} = 0$). This fact can be explained by dressed-mode theory. Resonant cavity–QD interaction results in two dressed modes, which are significantly detuned from the second *empty* cavity with the detuning $\pm|g_1(\vec{r})| = \pm\Gamma/2$. Both dressed modes non-resonantly couple with the empty mode, resulting in two transparency peaks located at frequencies $\omega \approx \pm\Gamma/4$. When $\delta_{21} = \Gamma/2$, one dressed cavity mode non-resonantly couples with the empty mode with a detuning Γ, which leads to a transparency peak located near $\omega \simeq 0$, while the other dressed mode resonantly couples with the empty mode, which does not result in a transparency peak. When δ_{21} continually increases, e.g. $\delta_{21} = \Gamma$, the vanished peak reappears since the two dressed modes are always non-resonant with the empty mode.

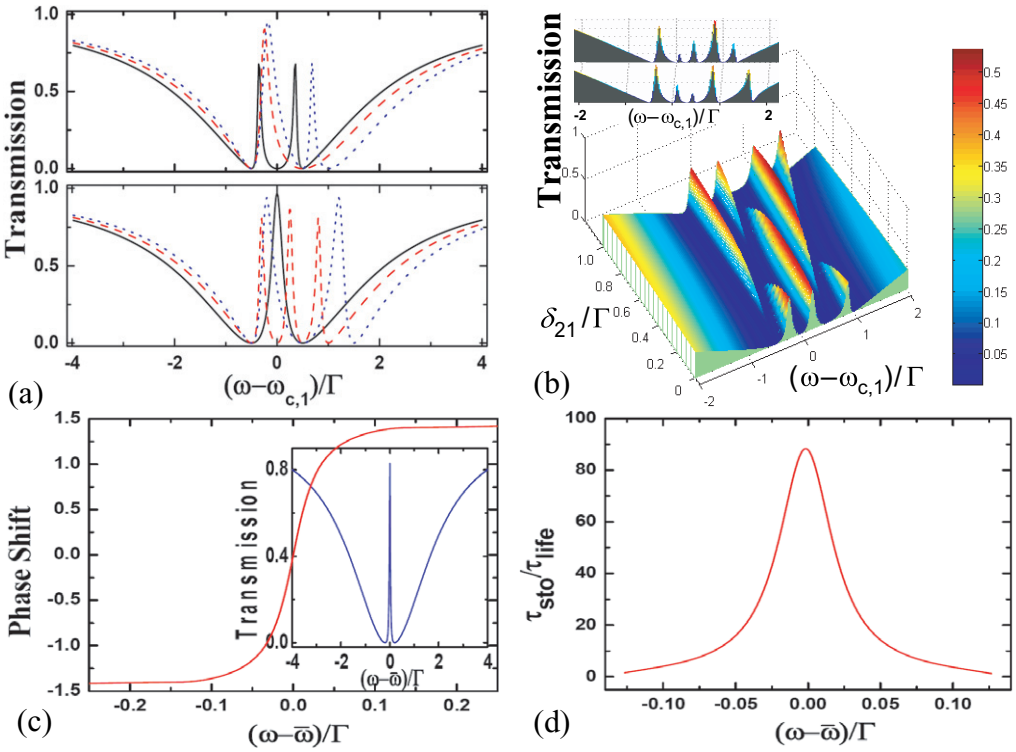

Figure 3. (a) Transmission spectra of two coupled subsystems with one QD (top) and two QDs (bottom) where $g = \Gamma/2$ and $\gamma = \gamma_1 = \gamma_2 = \kappa_0$. Other conditions are the same as in figure 2(a). (b) Spectral character of three coupled subsystems with $\delta_{31} = \Gamma/2$ and $\delta_{1,2,3} = 0$. Inset: $\delta_{31} = \Gamma/2$, $\delta_{21} = 0$, $\delta_1 = \delta_3 = 0$, with $\delta_2 = \Gamma/2$ (top) and $\delta_2 = \Gamma$ (bottom). (c) and (d) Photon phase shift and delay (τ_{sto}) through two QD–cavity subsystems, where $\omega_{c(r),j} = \varpi$ and $g = 0.2\Gamma$. Inset: transmission spectrum.

Figure 3(a) (bottom) illustrates the case where both cavities resonantly interact with a single QD each. Similar to the above analysis, we can explain the number and locations of sharp peaks with respect to different δ_{21} by comparing the two pairs of dressed modes. For example, when $\delta_{21} = \Gamma$, the dressed modes in the first cavity are located at $\pm\Gamma/2$, whereas the second pair is at $\Gamma/2$ and $3\Gamma/2$, so the transparency peaks are located at $[-\Gamma/2, \Gamma/2]$ and $[\Gamma/2, 3\Gamma/2]$, i.e. two peaks are near 0 and Γ. Figure 3(b) shows the spectral character of three coupled cavity–QD subsystems, under various cavity–cavity and cavity–QD detunings. These transmission characteristics are helpful during experimental realization efforts to identify the required tunings and detunings when multiple QD transitions and cavity resonances are involved.

3.1. Phase shift and photon storage

To further examine this coupled cavity–QD system, figure 3(c) shows the transmission phase shift for various detunings of the input photon central frequency, where the cavity and QD transition are resonant for both subsystems. The phase shift has a steep change as we had

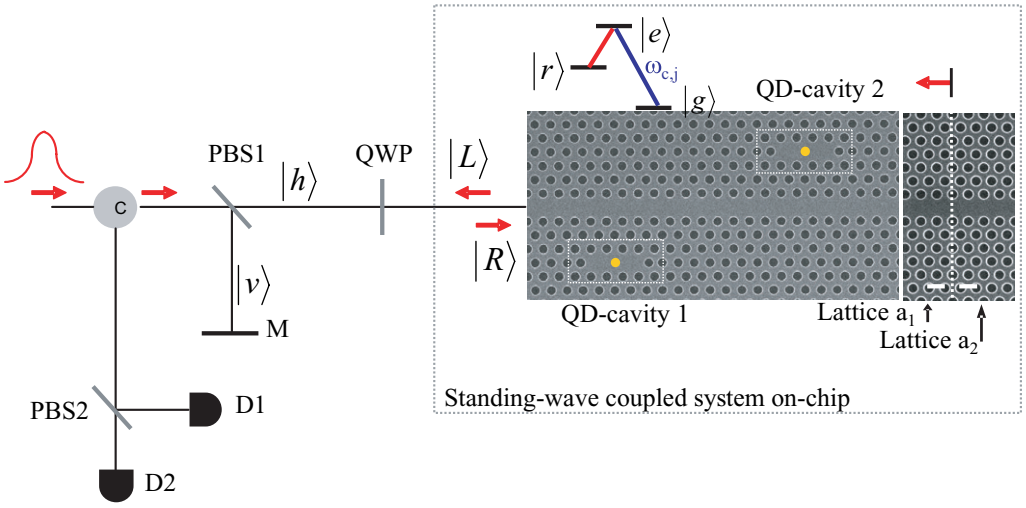

Figure 4. Schematic diagram to illustrate the two-qubit quantum phase gate based on the coupled cavity–cavity multi-QD scheme. A heterostructure reflection element is introduced at the end of the waveguide to remove spatial mode distinguishability, with only a single-output mode $|L\rangle$ for an input photon mode $|R\rangle$. The QDs have a superposition of two ground states, $|g\rangle$ and $|r\rangle$. PBS1 and PBS2 represent the polarization beam splitters, D1 and D2 the single-photon detectors, C the circulator and M the reflecting mirror. Here, PBS1 and PBS2 are actually regarded as filters since only the *h*-polarized photon is required in our scheme. The response of detectors D1 and D2 provide an indication to show the success of the gate operation and can also be used for measurement-induced entanglement in future.

expected intuitively, which corresponds to a strong reduction of the group velocity of the photon. As shown in figure 3(d), the delay time ($\tau_{\rm sto}$) in this coupled system is almost a hundred times the cavity lifetime ($\tau_{\rm life} = 1/2\Gamma$). This coupled cavity–QD system can essentially be applied to the storage of the photon. Moreover, our solid-state implementation has an achievable bandwidth of ~50 MHz in contrast to less than 100 kHz in atomic systems, although the delay-bandwidth product is comparable. To obtain longer photon storage, one can consider dynamical tuning [29] to tune the cavity resonances with respect to the QD dipolar transitions to break the delay-bandwidth product in a solid-state cavity–QD array system.

4. Quantum phase gate operation

In the above section, we have shown the novel transport character of the coupled cavity–QD system. Now we study the possibility of quantum phase gate operation of the QDs based on this transport character. The scheme to realize this multi-QD coupled cavity–cavity system is illustrated in figure 4. The QDs are represented by two ground states $|g\rangle$ and $|r\rangle$, where the state $|r\rangle$ is largely detuned with the respective cavity mode. The two ground states can be prepared via QD spin states as demonstrated remarkably in experiment in [30] with near-unity fidelity. The input weak photon pulse is assumed *h*-polarized, with an input pulse duration *D*

(e.g. 1 ns) larger than the loaded cavity lifetime for the steady-state approximation. To remove the distinguishability of the two output photon spatial modes in the waveguide (transmitted and reflected), a reflecting element is inserted at the end of the waveguide (such as a heterostructure interface [17, 18]), as shown in figure 4. This ensures that the photon always exits in the left-propagating mode $|L\rangle$ (from a right-propagating input mode $|R\rangle$) without any entanglement with the QD states. Alternatively, a Sagnac interferometer scheme such as introduced in [31] can also be implemented to remove the spatial mode distinguishability and QD–photon entanglement. In this single-input single-output mode scheme [32, 33], $|h\rangle$ and $|v\rangle$ represent the two polarization states of the input photon. We emphasize that in the below calculations we have considered the complete characteristics of the full system (including the end reflecting element and the resulting 'standing wave' due to the long photon pulse width) where we examined the final left-propagating output mode $|L\rangle$ from a right-propagating input mode $|R\rangle$ (figure 4). The reflection interference is included where we force $\hat{b}_{\rm in}^{(2)} = \hat{b}_{\rm out}^{(2)}$ (figure 1(b)) from the reflection element, when calculating the temporal pulse delays for the different QD states.

To facilitate the discussion but without loss of generality, we describe the all resonance case (i.e. $\omega = \omega_{{\rm c}(r),j}$) to describe the idea of the phase gate operation; in the subsequent numerical calculations, we will demonstrate the gate feasibility under non-ideal detunings. As an example, we focus on the realization of a two-qubit (two QDs) phase gate. Figure 5 now shows the calculated reflection field (real and imaginary components) of the complete coupled cavity–cavity and two-QD system for the four superpositioned states: $|\Psi\rangle = \alpha_1|r\rangle_1|r\rangle_2 + \alpha_2|g\rangle_1|r\rangle_2 + \alpha_3|r\rangle_1|g\rangle_2 + \alpha_4|g\rangle_1|g\rangle_2$. We address the following cases for the different QD states.

- Case I. The two QDs are initially prepared in $|u\rangle_1|v\rangle_2 (u, v = g, r)$ and at least one QD occupies the ground state $|r\rangle$. From figures 5(a) and (b) and for the all resonance case, we see that ${\rm Re}[r_{21}] \simeq -1$ and ${\rm Im}[r_{21}] \simeq 0$ under the over-coupling regime ($\kappa_0 \ll \kappa_1$) and with the large Purcell factor ($g^2/\Gamma\gamma \gg 1$). This fact can be understood by regarding the resonant condition ($\omega_{c,j} = \omega$). The input photon will be almost reflected by one *empty* cavity, in which the QD is in $|r\rangle$, resulting in a final state $-|u\rangle_1|v\rangle_2|L\rangle$.
- Case II. The QDs initially occupy $|g\rangle_1|g\rangle_2$. In this case, note that the photon pulse interacts coherently with both cavities and two QDs, including the reflection element that is placed specifically to achieve $\hat{b}_{\rm in}^{(2)} = \hat{b}_{\rm out}^{(2)}$, before completely exiting the system. As demonstrated in figures 5(a) and (b) and for the all resonance case, the final output state is described by ${\rm Re}[r_{21}] \simeq 1$ and ${\rm Im}[r_{21}] \simeq 0$. The resulting state is $|g\rangle_1|g\rangle_2|L\rangle$. We note that the photon loss is small for all four cases when the input photon pulse is in resonance with the cavity resonances, as can be done experimentally by tuning the input photon.

Therefore, with the exit of the photon of the single-input single-output system, the state of the two QDs after the interaction is now described by: $|\Psi\rangle = -\alpha_1|r\rangle_1|r\rangle_2 - \alpha_2|g\rangle_1|r\rangle_2 - \alpha_3|r\rangle_1|g\rangle_2 + \alpha_4|g\rangle_1|g\rangle_2$. Hence, after the above process and recombining at PBS1, the state of the QD–QD gate described by $U = {\rm e}^{{\rm i}\pi|g\rangle_{12}\langle g|}$ can be manipulated. Moreover, if $\alpha_i = 1/2\,(i = 1, 2, 3, 4)$, we have $|\Psi\rangle = 1/\sqrt{2}(|r\rangle_1|-\rangle_2 + |g\rangle_1|+\rangle_2)$ (where $|-\rangle_2 = 1/\sqrt{2}(|g\rangle_2 - |r\rangle_2)$ and $|+\rangle_2 = 1/\sqrt{2}(|g\rangle_2 + |r\rangle_2)$), which is the generation of the maximally entangled state in the coupled QDs. Most importantly, this idea can also be extended to realize an N-qubit gate with only one step, which is of importance for reducing the complexity of practical quantum computation and quantum algorithms for physical realization. In addition, using this configuration, some special entangled QD states (e.g. the cluster state) can be generated [34].

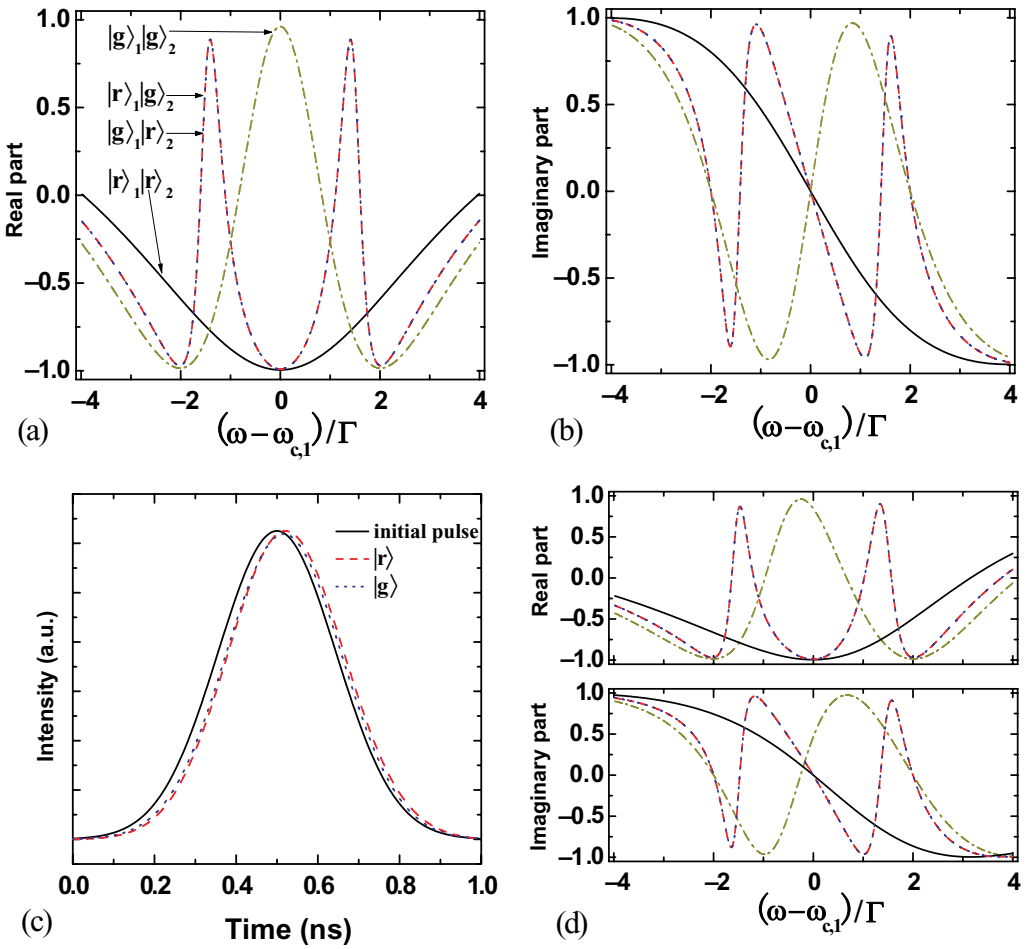

Figure 5. Real (a) and imaginary (b) parts of the reflection coefficients for initial QD states, $|r\rangle_1|r\rangle_2$, $|r\rangle_1|g\rangle_2$, $|g\rangle_1|r\rangle_2$ and $|g\rangle_1|g\rangle_2$. Here, we assume $|g_1(\vec{r})| = |g_2(\vec{r})| = 2\Gamma$, $\delta_{21} = \delta_1 = \delta_2 = 0$, and the propagation phase between the second cavity and the reflection element is adjusted as $\theta' = n\pi + \pi/2$ to compensate for the phase shift induced by the mirror reflection (ideally, π). Other parameters are the same as in figure 2(a). (c) Shape function of the photon pulse for cases when the single QD is coupled ($|g\rangle$) or decoupled ($|r\rangle$) to the single cavity, and without the cavity. (d) Real and imaginary parts of the reflection coefficient when the reflection phase of the mirror deviates from ideal π with a deviation of 0.5.

We provide a few more notes on the designed coupled cavity–cavity multi-QD system. Firstly, the temporal distinguishability is small for the single cavity–QD system; in figure 5(c), we plot the shape function of the output photon pulse for cases when the QD is coupled ($|g\rangle$), decoupled ($|r\rangle$) or without the cavity, through numerical simulation of the dynamical evolution of the system. The pulse shape function overlaps very well. Secondly, the calculated temporal distinguishability in the coherently coupled cavity–cavity multi-QD system is also small compared with the pulse duration D. Specifically, with the parameters in figure 5(a), the photon delays due to the coupling to the cavities are calculated as approximately τ_{life}, $2\tau_{\text{life}}$,

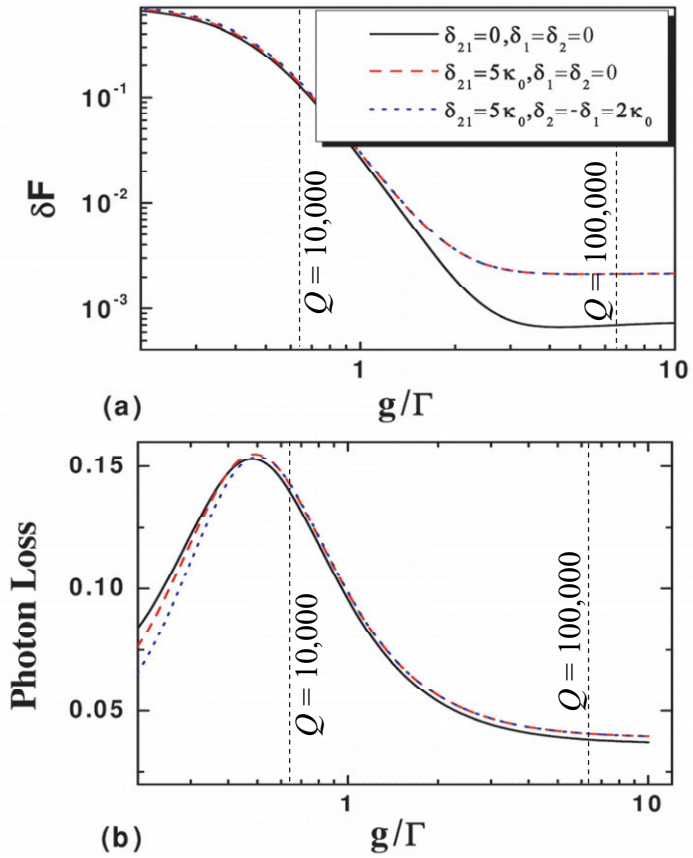

Figure 6. Gate fidelity change ($\delta F \equiv 1 - F$) (a) and photon loss P (b) of the two-qubit gate versus g/Γ. The reflecting element has 95% reflectivity. Here the carrier frequency is assumed as $\varpi - 2.5\kappa_0$ to avoid the EIT-like peaks of two coupled empty cavities, and a scattering loss of 1% is used for the short propagation lengths. Other parameters are the same as in figure 3(a). The shaded areas correspond to loaded cavity Q values in the range of 10^4 to 10^5.

$2\tau_{\text{life}}$ and $4\tau_{\text{life}}$ in the case of the states $|r\rangle_1|r\rangle_2$, $|r\rangle_1|g\rangle_2$, $|g\rangle_1|r\rangle_2$ and $|g\rangle_1|g\rangle_2$, respectively, where the loaded cavity τ_{life} is about 0.02 ns. The photon delay of the complete system is therefore sizably smaller than the pulse duration (of 1 ns, for example). Furthermore, this cavity-induced delay will furthermore decrease with increasing the coupling rate g, further reducing temporal distinguishability. Of course, the size of the chip is also small (tens of microns) so that the propagation time ($2S/v$, where S denotes the distance between the first cavity and the reflector, and v the group velocity) in the waveguide is much smaller than the pulse duration D. Thirdly, we examine the dependence of the overall system reflection coefficient on the phase variation from the reflection element, when deviating from the ideal π phase shift. Figure 5(d) shows the numerical results, where a slight dependence is observed when there is a phase deviation of 0.5 from π. Moreover, the phase shift from the reflection element can be externally controlled stably, e.g. with an external and focused pump beam to thermally tune the reflection region.

5. Gate fidelity and photon loss

To exemplify the coupled cavity system, isolated single semiconductor QDs in high-Q small modal volume (V) photonic crystal cavities are potential candidates, such as self-assembled InAs QDs in GaAs cavities [20]–[23], or PbS nanocrystals in silicon cavities at near 1550 nm wavelengths [35]. For the PbS nanocrystal and silicon cavity material system, we use the following parameters in our calculations: $\gamma_s \sim 2$ MHz, $\gamma_p \sim 1$ GHz at cooled temperatures, $V \sim 0.4\,\mu m^3$ at 1550 nm, with a resulting single-photon coherent coupling rate of $g \sim 12.4$ GHz. Loaded cavity Q values in the range of 10^4 and 10^5 are achievable experimentally, with intrinsic Q values up to 10^6 reported recently [18, 19].

To characterize the present gate operation, figures 6(a) and (b) present the two-qubit phase gate fidelity F and photon losses P for various g values and the parameters described above, even under non-ideal detuning conditions and the bad cavity limit. It should be noted here that, with δ_{21} and $\delta_{1,2}$, we can know the detuning between two QDs. For example, in the case of $\delta_{21} = 5\kappa_0$ and $\delta_{1,2} = 0$, we deduce that the detuning between the two QDs is $5\kappa_0$. Based on the above parameters, F can reach 0.99 or more, and P can be below 0.04. As shown in figure 6, for cavity–cavity detunings in the range of the intrinsic cavity decay rate, both F and P do not degrade significantly but are strongly dependent on the cavity decay rate. Likewise, with QD–cavity detuning that is comparable with the intrinsic cavity decay rate, both F and P do not change significantly but are dependent on the cavity decay rate. We note that the on-resonant (the cavity modes are resonant with the dipole transitions of the QDs) photon loss P can be larger than the non-resonant case when g is small. This can be explained by considering the decay of QDs. When the QDs resonantly interact with cavity modes, the decay of QDs becomes distinct, resulting in an increase of photon loss. Moreover, we note that the QD–QD detuning plays an important role in the quantum gate operations. Given the current large inhomogeneous distribution of QD transitions, however, active tuning methods such as Stark shifts would probably be needed to control the detuning within acceptable bounds to obtain a strong quantum gate fidelity and a low photon loss. Furthermore, we note that, with increasing g, the photon loss P exhibits an increase before a decrease, which can be understood by studying the photon loss when the QDs are in the state of $|g\rangle_1|g\rangle_2$. When $g \simeq \Gamma/2$, the absorption strength (resulting from κ_0 and γ) of the input photon by the coupled cavities reaches the maximum.

6. Conclusion

We proposed and investigated the operation and performance of a scalable cavity–QD array on a photonic crystal chip towards controlled quantum phase gates. The coupling among single-QD emitters and quantized cavity modes in a coherent array results in unique transmission spectra, with an optical analogue of EIT-like resonances providing potential photon manipulation. In the quantum phase gate operation, we note that the gate fidelity can reach 0.99 or more and the photon loss can be below 0.04 in a realistic semiconductor system, provided the non-ideal detunings are kept within the cavity decay rates. Our study provides an approach for a chip-scale two-qubit gate towards a potential quantum computing network [36, 37].

Acknowledgments

We thank F Sun for helpful discussions, and acknowledge funding support from the DARPA, the New York State Office of Science, Technology and Academic Research and the NSF.

YFX, XBZ, YLC, ZFH and GCG were also supported by Knowledge Innovation Project and International Partnership Project of the Chinese Academy of Sciences and by the Chinese Postdoctoral Science Foundation.

References

[1] Mabuchi H and Doherty A C 2002 *Science* **298** 1372
[2] McKeever J *et al* 2003 *Phys. Rev. Lett.* **90** 133602
[3] Keller M *et al* 2004 *Nature* **431** 1075
McKeever J *et al* 2004 *Nature* **303** 1992
Kuhn A, Hennrich M and Rempe G 2002 *Phys. Rev. Lett.* **89** 067901
[4] Volz J *et al* 2006 *Phys. Rev. Lett.* **96** 030404
[5] Rosenfeld W *et al* 2007 *Phys. Rev. Lett.* **98** 050504
[6] Smith D D *et al* 2004 *Phys. Rev.* A **69** 063804
[7] Xiao Y-F *et al* 2007 *Phys. Rev.* A **75** 063833
Qian J, Qian Y, Feng X-L, Jin S-Q and Gong S-Q 2008 *Phys. Rev.* A **77** 023823
[8] Xu Q *et al* 2006 *Phys. Rev. Lett.* **96** 123901
[9] Totsuka K, Kobayashi N and Tomita M 2007 *Phys. Rev. Lett.* **98** 213904
[10] Cirac J I, Zoller P, Kimble H J and Mabuchi H 1997 *Phys. Rev. Lett.* **78** 3221
Yao W, Liu R B and Sham L J 2005 *Phys. Rev. Lett.* **95** 030504
Serafini A, Mancini S and Bose S 2006 *Phys. Rev. Lett.* **96** 010503
[11] Ogden C D, Irish E K and Kim M S 2008 arXiv:0804.2882
[12] Hartmann M J, Brandao F G S L and Plenio M B 2006 *Nat. Phys.* **2** 849
Hartmann M J and Plenio M B 2007 *Phys. Rev. Lett.* **99** 103601
[13] Greentree D, Tahan C, Cole J H and Hollenberg L C L 2006 *Nat. Phys.* **2** 856
Angelakis D G, Santos M F and Bose S 2007 *Phys. Rev.* A **76** 031805
[14] Hartmann M J, Brandao F G S L and Plenio M B 2007 *Phys. Rev. Lett.* **99** 160501
[15] Hughes S 2007 *Phys. Rev. Lett.* **98** 083603
[16] Hu F M, Zhou L, Shi T and Sun C P 2007 *Phys. Rev.* A **76** 013819
[17] Tanaka Y, Upham J, Nagashima T, Sugiya T, Asano T and Noda S 2007 *Nat. Mater.* **6** 862
[18] Noda S, Fujita M and Asano T 2007 *Nat. Photonics* **1** 449
[19] Tanabe T, Notomi M, Kuramochi E, Shinya A and Taniyama H 2007 *Nat. Photonics* **1** 49
[20] Yoshie T *et al* 2004 *Nature* **432** 200
[21] Hennessy K *et al* 2007 *Nature* **445** 896
[22] Englund D *et al* 2007 *Opt. Express* **15** 5550
[23] Badolato A *et al* 2006 *Science* **308** 1158
[24] Englund D *et al* 2007 *Nature* **450** 857
[25] Xiao Y-F *et al* 2007 *Appl. Phys. Lett.* **91** 151105
[26] Waks E and Vuckovic J 2006 *Phys. Rev.* A **73** 041803
[27] Sørensen A S and Mølmer K 2003 *Phys. Rev. Lett.* **91** 097905
[28] Ghose R N 1963 *Microwave Circuit Theory and Analysis* (New York: McGraw-Hill)
Slater J C 1950 *Microwave Circuits* (New York: McGraw-Hill)
Kurokawa K 1969 *An Introduction to the Theory of Microwave Circuits* (New York: Academic)
[29] Yanik M F, Suh W, Wang Z and Fan S 2004 *Phys. Rev. Lett.* **93** 233903
Xu Q, Dong P and Lipson M 2007 *Nat. Phys.* **3** 406
Yanik M F and Fan S 2007 *Nat. Phys.* **3** 372
[30] Atatuer M *et al* 2006 *Science* **312** 551
[31] Gao J, Sun F and Wong C W 2008 *Appl. Phys. Lett.* **93** 151108

[32] Duan L-M, Wang B and Kimble H J 2005 *Phys. Rev.* A **72** 032333
Duan L-M and Kimble H J 2004 *Phys. Rev. Lett.* **92** 127902
Duan L-M, Kuzmich A and Kimble H J 2003 *Phys. Rev.* A **67** 032305
[33] Lin X-M, Zhou Z-W, Ye M-Y, Xiao Y-F and Guo G-C 2006 *Phys. Rev.* A **73** 012323
[34] Cho J and Lee H-W 2005 *Phys. Rev. Lett.* **95** 160501
[35] Bose R *et al* 2007 *Appl. Phys. Lett.* **90** 111117
[36] Cirac J I, Zoller P, Kimble H J and Mabuchi H 1997 *Phys. Rev. Lett.* **78** 3221
[37] Serafini A, Mancini S and Bose S 2006 *Phys. Rev. Lett.* **96** 010503